Chem. Chem. Technol., 2023,
Vol. 17, No. 4, pp. 758–765

Chemistry

CRYSTAL SMECTIC G PHASE RETARDER FOR THE REAL-TIME SPATIAL-TEMPORAL MODULATION OF OPTICAL INFORMATION

Gia Petriashvili[1,✉], Andro Chanishvili[1], Nino Ponjavidze[1], Ketevan Chubinidze[1], Tamara Tatrishvili[2,3], Elene Kalandia[1], Ana Petriashvili[1], Tamar Makharadze[1]

https://doi.org/10.23939/chcht17.04.758

Abstract. We have manufactured and investigated a novel phase retarder based on a rare and less studied liquid crystal phase, such as the Crystal Smectic G-phase prepared by mixing two certified nematic mixtures. The phase retarder is transparent in the visible and near-infrared parts of the optical spectrum. The temperature stability over a wide temperature range, high birefringence, and high strength, allow the production of various types of phase retarders that can be used in optics, optical chemical analysis, and polarimetry.

Keywords: Crystal Smectic G phase, phase retarder, optical information.

1. Introduction

Phase retarders or wave-plates are the birefringent optical devices used to modulate the phase of polarized light in bulk optical systems. The most common polarization modulators act as converters between linear and circular polarization states and between linear polarization states with different directions of linear polarization. The change in retardation can be achieved by changing the optical thickness in a birefringence crystal[1], using piezoelectric mirrors, by changing the birefringence of a material,[2] and in Pockels/Kerr cells.[3] Phase retardance is expressed in units of length, waves, degrees, or radians. The most common types of wave plates are quarter-wave plates ($\lambda/4$ plates) and half-wave plates ($\lambda/2$ plates), where the difference of phase delays between the two linear polarization directions is $\pi/2$ or π, corresponding to propagation phase shifts over a distance of $\lambda/4$ or $\lambda/2$. Since the birefringence of commonly available crystals is weak, conventional wave plates usually have a large physical thickness to obtain the desired phase retardation, which greatly hinders the miniaturization of bulky wave plates and restricts the development of on-chip optics and photonics integration.[4] Due to their low cost, absence of moving parts, low driving voltage, and small sizes, the liquid crystals (LCs) are outstanding candidates for use in phase modulators as they exhibit a broadband birefringence (Δn), a giant optical nonlinearity and a transparent spectral region from 400 nm to 20 μm. LC-based polarization modulation is used in various optical devices for beam steering, spatial light modulation, imaging Stokes polarimetry, optical switching, and display applications. This technology provides important benefits for other typical retarders or phase shifters.[5-18] However, the retardance based on nematic LC strongly depends on an ambient temperature.[19] Besides, most LC materials absorb the UV part of the optical spectrum, resulting in quick degradation. Smectic liquid crystals (SmLCs) are materials formed by stacking deformable, fluid layers. SmLCs have a wide variation from low-ordered Sm phases to highly ordered Sm phases, which are often called Sm A, Sm B, Sm C, *etc.*, according to the historical order of their discovery, and are all characterized by the layered structure of LC molecules. Each SmLC phase, however, has a different molecular orientation and alignment in an Sm layer. The Sm phases, such as Sm B, Sm E, Sm I, Sm J, and Sm G, have interconnections between the molecular layers in a limited range, so they are sometimes classified as crystals.[20] In the present study, we have prepared a crystal Sm G (CSm G) phase and demonstrated for the first time that this state of the LC phase acts as a phase retarder with spectral and polarization characteristics independent of temperature in a wide temperature range.

[1] Vladimir Chavchanidze Institute of Cybernetics of the Georgian Technical University, 5 Z. Andjzaparidze St., Tbilisi, 0186, Georgia
[2] Ivane Javakhishvili' Tbilisi State University, Department of Macromolecular Chemistry, 1 I. Chavchavadze Ave., Tbilisi, 0179, Georgia
[3] Institute of Macromolecular Chemistry and Polymeric Materials, Ivane Javakhishvili Tbilisi State University, 1 I. Chavchavadze Ave., Tbilisi, 0179, Georgia
✉ *g.petriashvili@yahoo.co.uk*

2. Experimental

2.1 Materials and Sample Preparation

The CSm G LC mixture was prepared by mixing ZLI-1184 and ZLI-1185 (the nematic matrices) with a ratio of 1:1, w/w. Both materials were purchased from Merck. The prepared mixture was stirred in the isotropic phase at ~90 °C for ~25 min to make the constituents uniformly mixed. To implement the CSm G-based phase retarder and to investigate the retardation behavior of the resulting substance, we assembled a planar optical cell using two quartz plates of 30 x 30 x 1 mm in size. It is known from the literature that polymeric binders are one of the most vital components of organic coatings because they serve as a material that integrates with the other components, allowing the improvement in the adhesion properties of the thin-layer coatings.[21-23] For this purpose, we used a solution composed of 99.4% water + 0.6 % polyvinyl alcohol (PVA) as a coating layer. The prepared solution was deposited on the quartz substrates by spin-coating and then rubbed to obtain planar alignment of the LC material. The spacing between the quartz plates was fixed, using the Mylar films with different thicknesses. The prepared mixture was capillary infiltrated into the optical cell.

2.2. Methods

To study the optical, thermal, and photo-optical properties of the prepared CSm G phase, a method of optical spectral analyses was used. The polarizing digital microscope was used for the estimation of the CSm G structure homogeneity. The optical polarized microscope coupled to a fiber-optic spectrometer (Avaspec-2048, "Avantes") and a high-resolution CCD camera was used as the imaging-based technique for the visual and graphical presentation of the information of the transmitted light through the optical cell. A hot stage with 0.1 °C accuracy was used to control the optical cell temperature. The Abbe refractometer served for the measurement of the refractive index values at different wavelengths.

2.3. Formation and Thermo-Optical Properties of CSm G Phase

There are a number of Sm LCs, characterized by the variety of molecular arrangements within the layers, which vary from low-ordered Sm phases to highly-ordered ones. For example, in the Sm B and E phases, the molecular long axes are essentially parallel to the normal layer planes, while in the Sm G, H, J, and K phases, they are tilted to the layer normals. Originally these phases were designated as smectics, but further investigations have demonstrated their three-dimensional character, which has an interaction between the molecular layers in a limited range, so they are sometimes classified as crystals.[24] Here we note that the LC mixture prepared by us is a CSm G phase, which is confirmed by several facts. In contrast to the Sm A and B phases, in which the optical axis is perpendicular to the Sm layers, the optical axis of the CSm G phase is inclined to the Sm layers. Moreover, the molecules in the CSm G phase exhibit a hexagonal positional arrangement, and the viscosity is significantly high so the glass plates of the optical cell cannot move, indicating a long translational order of the layers to each other. In addition, the prepared Sm phase has a very similar texture to the textures of the CSm G phases described in the literature.[25-28] Using a spectrometer, we recorded an absorption spectrum of the prepared LC mixture in its isotropic phase and found that it is optically transparent starting from λ=270 nm. To determine the temperature-dependent phase transitions the LC mixture was capillary infiltrated into 12 μm optical cells. Then an optical cell was embedded in the hot stage and placed under an optical microscope coupled to a spectrometer. The temperature dependencies of the phase transitions recorded during cooling and heating are demonstrated in Fig. 1. The sequence of phase transition temperatures during heating and cooling is equal to each other.

Fig. 1. Temperature-dependent phase transition of ZLI-1184 + ZLI-1185 substance during cooling and heating

As shown in Fig. 1, the temperature interval of the CSm G phase is wide, equal to 71.8 °C. Under the optical polarized microscope, the CSm G phase has a mosaic structure. Inside each cluster, molecules have a determined direction so that the optical axis of each one to the other has a random orientation. We found that each domain merges with another over time and transforms into a single uniaxial optical crystal when the optical cell was placed in a hot stage at 35 °C for 48 hours. The image in Fig. 2 shows the transformation of a mosaic multi-domain texture of the CSm G phase into a single and large CSm G domain with one optical axis with a well-determined direction.

From the moment of formation of a large area of the CSm G phase, it retains a homogeneous state over the entire temperature range of the phase existence. Next, we measured the wavelength-dependent refractive changing of indices of the obtained structure using an Abbe refractometer. Fig. 3 shows the wavelength-dependent extraordinary n_e and ordinary n_o refractive indices of the uniaxial CSm G phase at fixed room temperature.

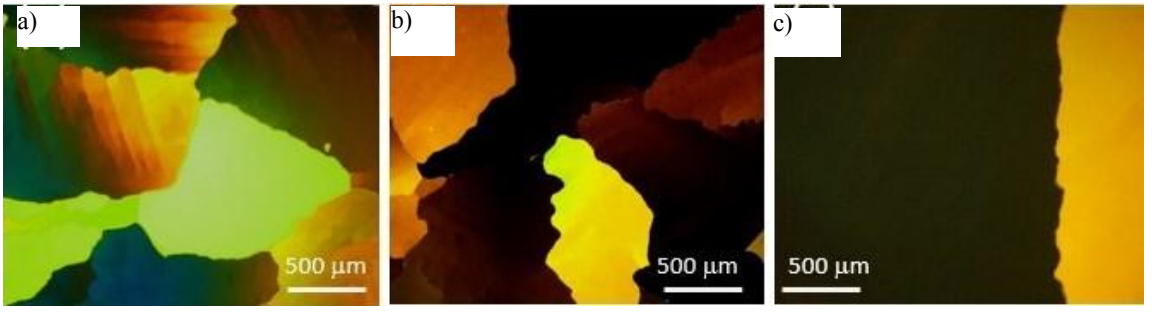

Fig. 2. Time-dependent transformation of the CSm G phase from the initial mosaic multi-domain textures (a, b) into the final single-domain uniaxial one (c)

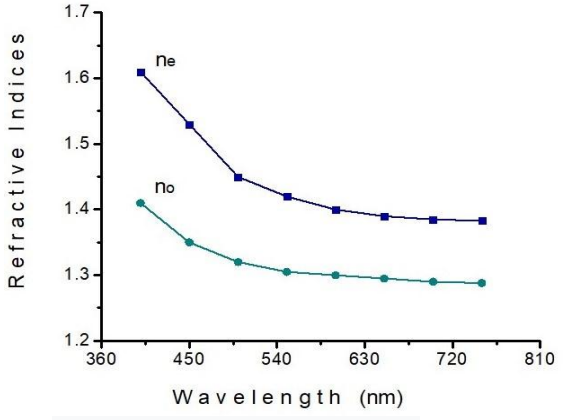

Fig. 3. Refractive indices vs. wavelength for uniaxial CSm G phase at room temperature

3. Results and Discussion

Due to the high birefringence of the CSm G material, the optical cell filled with CSm G substance acts as an optical phase retarder, with its optical axis parallel to the surface of the retarder. The experimental setup of the CSm G-based phase retarder is shown in Fig. 4. White light from a tungsten lamp passes through a collimating lens and then crosses a linear polarizer oriented at 45° relative to the optical axis of the retarder. The orthogonal polarization components pass through the material at different velocities (due to birefringence) and are phase-shifted relative to each other, which forms modified polarization states. After passing through the analyzer and a focusing lens, the emerging signal is collected by an optical fiber spectrometer coupled to the computer.

The phase retardation, Γ, is given by the following expression,

$$\Gamma = 2\pi((n_e - n_o)L/\lambda) \qquad (1)$$

where L is the thickness of the CSm G phase retarder, λ is the wavelength, and n_o and n_e are the refractive indices of *o*-light and *e*-light, respectively. This Eq. (1) describes that retardance strongly depends upon incident wavelength, material birefringence, and phase retarder thickness. Retarders can be multiple-order, having several waves of retardance. The spectral-dependent retardation of the multiple-order phase retarder, assuming the perpendicular incidence of the beam on the wave plate, is given by

$$\Gamma(\lambda, \Delta n) = 2\pi L \int_{\lambda_m}^{\lambda_n} [(n_e - n_o)/\lambda] d(\lambda) \qquad (2)$$

where λ_m and λ_n correspond to the initial and final spectral positions of the wavelengths. Fig. 5 shows the multi-wave phase retardation produced by CSm G phase retarders. In particular, Fig. 5(a) displays the white light phase retardation produced by the CSm G retarder with 24 µm thickness, and Fig. 5(b) shows the white light phase retardation produced by a CSm G retarder with 100 µm thickness. The fabricated phase retarders act as polychroic filters with a comb-like design having multiple polarization-dependent variable transmission bands separated by multiple polarization-dependent absorption bands.

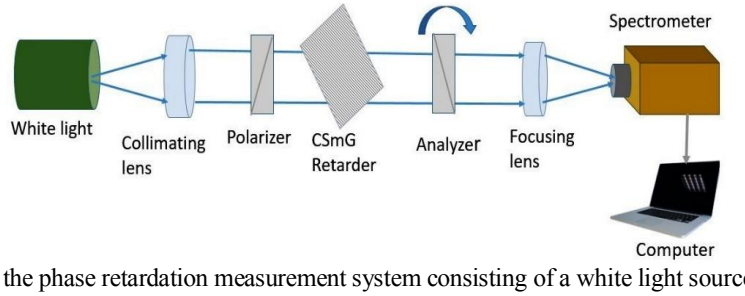

Fig. 4. Schematics of the phase retardation measurement system consisting of a white light source, a collimating lens, a polarizer, a CSm G phase retarder, an analyzer, a focusing lens, and a spectrometer coupled to the computer

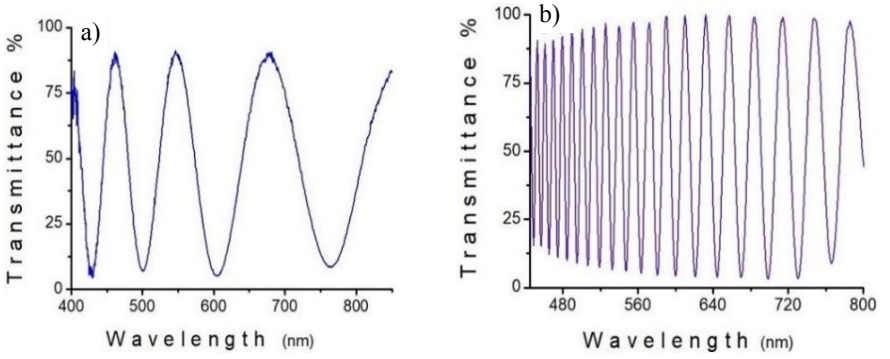

Fig. 5. Transmittance spectra of the 24 μm thick and 100 μm thick CSm G phase retarders as a function of the incident light wavelength

We have investigated the temperature-dependent phase retardation of the prepared CSm G phase retarder. For this purpose, an optical cell with 100 μm thickness was embedded in the hot stage. Starting from a temperature of +5.0 °C, the sample was heated up to 77.0±0.2 °C. After each temperature interval of 0.5 °C, the phase retardation was recorded graphically and compared to that recorded before. Converting the graphical data to the digital one, we obtained that in the given temperature interval of 5.0 ^{o}C–64.5 ^{o}C and the given spectral area of 400-800 nanometers, the temperature-dependent phase retardation was equal to zero as shown below

$$\Delta\Gamma(t,\lambda,\Delta n) = \\ = 2\pi L(\int_{ti}^{tj}\int_{\lambda m}^{\lambda n}\Delta n\partial(t)/\lambda\partial(t)) = \\ = 2\pi L(\int_{5.0^{o}C}^{64.5^{o}C}\int_{400nm}^{800nm}\Delta n\partial(t)/\lambda\partial(t)) = 0 \quad (3)$$

At the temperatures above 64.5 ^{o} C, the phase retardation becomes temperature-dependent with the increasing dependence and becomes maximum before the transition to the nematic phase. Using the CSm G-based phase retarder, we have demonstrated some examples of its application in optics and photonics.

3.1. Spatial-Temporal Modulation of Two Collinear Laser Beams

In this experiment, we used two CW-switched, He-Ne and Nd:YAG lasers demonstrating the spatial-temporal modulation of the laser emission when two laser beams propagate collinearly. A schematic of the experimental setup is shown in Fig. 6.

One of the two laser beams emitted by a 632 nm He-Ne laser passes through a half-silvered mirror, and the other, emitted by a 532 nm Nd:YAG laser, is reflected from the dielectric mirror and then reflected from a half-silvered mirror. The two beams were aligned as collinearly as possible. The two collinear beams then pass through a neutral density filter, a polarizer, a CSm G retarder, and an analyzer and are projected onto a screen. A CCD camera is used to spot the laser beams projected onto the screen. Since a standard CCD camera is sensitive to laser radiation, the beam images reflected from the screen are attenuated with a neutral density filter. The neutral density filter, the half-silvered, and the dielectric mirrors were selected so that the intensity of the laser beams was the same in each case. The laser light intensities at the screen surface were measured using an optical power meter (from Thorlabs). A spectrometer was used to record the modulation of the laser beam intensities. As shown in Fig. 7, when the polarizer and analyzer are crossed, the beam intensity emitted by the Nd:YAG laser is maximum, while the beam intensity emitted by the He-Ne laser is minimum, Fig. 7(a). Vice versa, when the polarizer and analyzer are aligned parallel, the beam intensity emitted by the Nd:YAG laser is minimum, and the beam intensity emitted by He-Ne is maximum, Fig. 7(b).

Fig. 8 demonstrates the images taken by a CCD camera. Fig. 8(a) shows the blend of red and green lights when both Nd:YAG and He-Ne laser beams are projecting onto the screen. Fig. 8(b) displays the highest intensity emitted by the Nd:YAG laser and Fig. 8(c) shows the maximum intensity emitted by the He-Ne laser.

3.2. Solar Spectral Radiation Division

In these experiments, we have shown that the CSm G phase retarder can be used as a comb-like optical filter that simultaneously and selectively transmits and absorbs different parts of the visible and near-infrared light emitted by the sun. For this purpose, we used the setup shown in Fig. 9, but in this case, the light received was solar radiation instead of the light emitted from an artificial light source. In this experiment, the optical fiber is pointed at the sun. A spectrometer was used to record the solar spectrum. First, the solar spectrum was recorded without using a CSm G phase retarder. Then, the CSm G phase retarder with 100 μm thickness was placed so that the linear polarizer aligned at a 45° angle to the optical axis of the retarder, and the solar spectrum was recorded again.

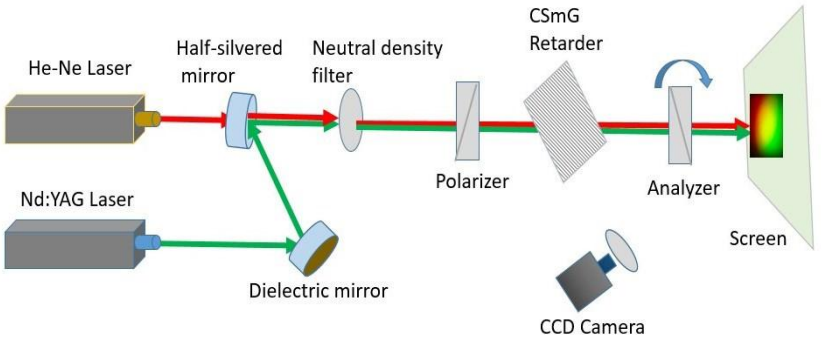

Fig. 6. Experimental setup to observe the spatial-temporal modulation of two collinear laser beams

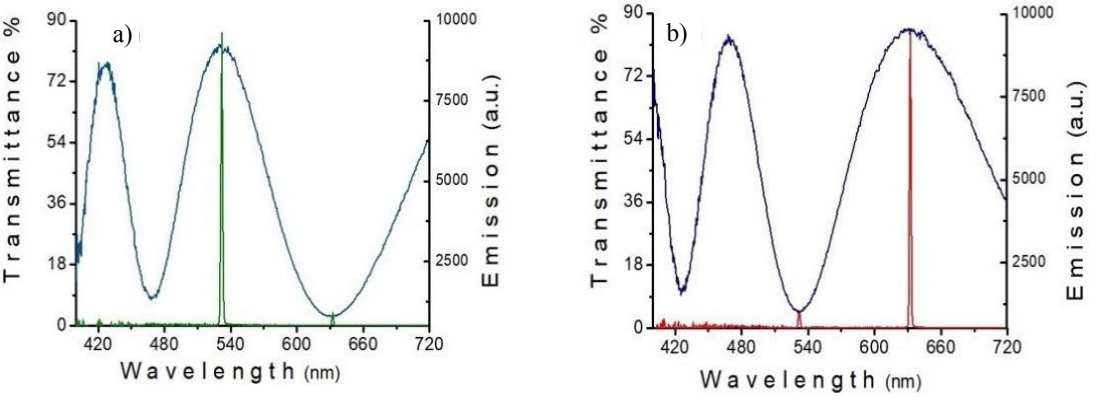

Fig. 7. Modulation of Nd: YAG (a) and He-Ne (b) lasers intensities produced by CSm G phase retarder

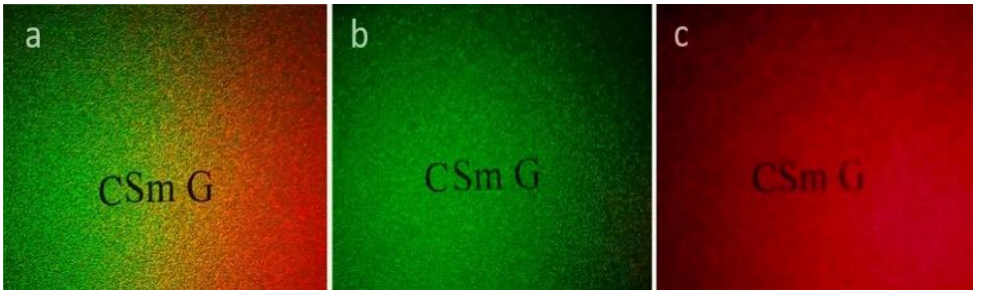

Fig. 8. Laser intensities modulation controlled by CSm G phase retarder

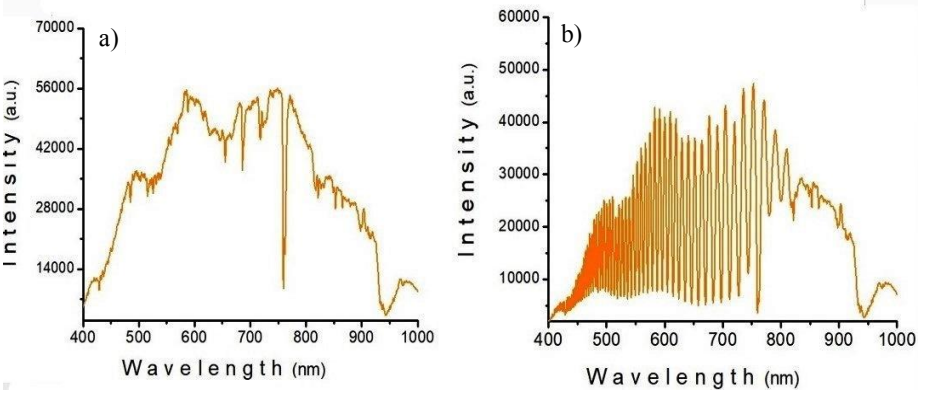

Fig. 9. The solar spectrum, recorded without (a) and with (b) CSm G phase retarder

Fig. 9(a) shows us the solar spectrum when no CSm G phase retarder was used, and Fig. 9(b) shows the solar spectrum when the beam passed through the CSm G phase retarder. Using a CSm G phase retarder, the solar spectrum was divided into small regions allowing us better distinguish the solar spectral lines, such as the Fraunhofer lines, and investigate the solar photosphere.

3.3. Aerospace Application

The blue color of the sky is caused by the scattering of sunlight by atmospheric molecules. This scattering, called Rayleigh scattering, is most effective at short wavelengths. Scattering by molecules and small particles, less than one-tenth of a wavelength is predominantly Rayleigh scattering. For particle sizes larger than one wavelength, Mie scattering predominates. Rayleigh scattering exhibits a strongly wavelength-dependent behavior. At 400 nm, the scattering is 9.4 times larger than at 700 nm for the same incident intensity. In addition, Rayleigh scattering is the most polarized, which increases the contrast between sky and clouds, because the light scattered by clouds is unpolarized. Since the CSm G-phase plate acts as a polarization-sensitive optical filter, we used it to enhance the image contrast of objects seen in the sky. For this purpose, we assembled an optical cell with a thickness of 12.5 μm. The optical cell was filled with a CSm G mixture and constructed as described above. A spectrometer was used to record the light transmittance as a function of wavelength at the different orientations of the analyzer. Fig. 10(a) shows the light transmittance when the polarizer and analyzer are crossed, and Fig. 10(b) shows the light transmittance when the polarizer and analyzer are aligned in parallel.

Next, the images of the clouds on a blue sky background are taken with a CCD camera. First, the image was captured without the CSm G-phase retarder and polarizers. Then, a setup was mounted so that the CSm G phase retarder was oriented at 45° to the polarizer. Fig. 11 shows images of the same section of sky, with Fig. 11(a) showing the image without polarizers and CSm G phase retarder, Fig. 11(b) demonstrates the case where the polarizer and analyzer have crossed, and Fig. 11(c) shows the image where the polarizer and analyzer are aligned in parallel.

Thus, a CSm-G phase retarder significantly improved the resolution quality of the objects in the sky background.

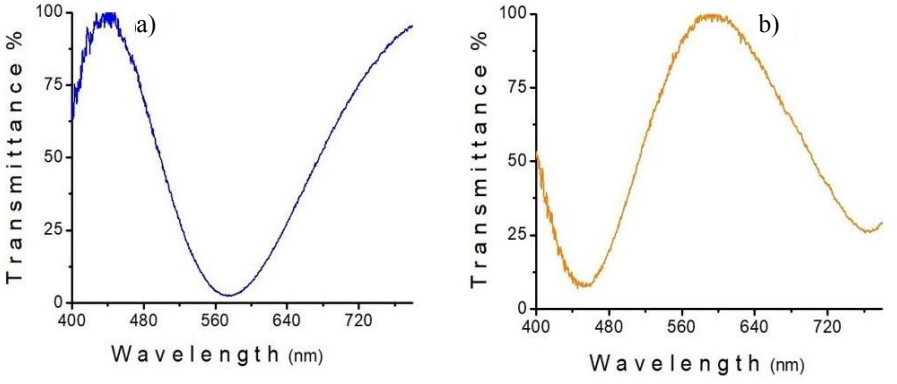

Fig. 10. Light transmittance through the CSm G phase retarder when the polarizer and analyzer are crossed (a) and when the polarizer and analyzer are aligned in parallel (b)

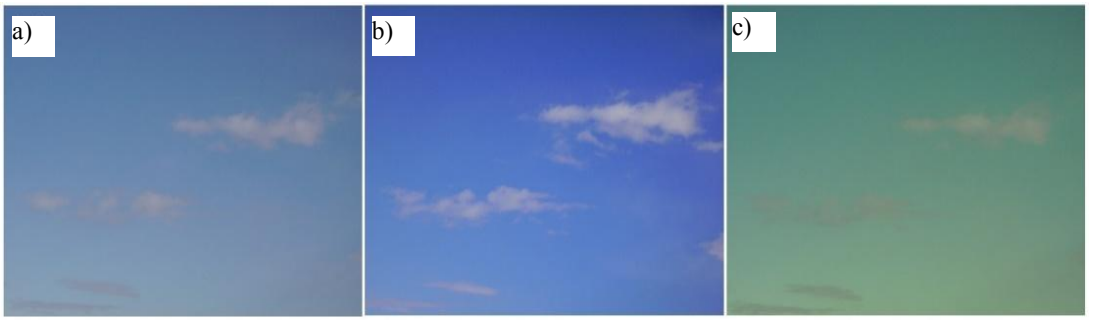

Fig. 11. The image of the same section of the sky: (a) without polarizers and a CSm G-phase retarder, (b) with crossed polarizer and analyzer, (c) with a polarizer and analyzer aligned in parallel

4. Conclusions

In summary, we prepared and investigated a CSm G phase and have shown for the first time that it can be used as an optical phase retarder. Mixing two nematic liquid crystals, a CSm G phase was obtained, and its temperature-dependent phase transitions were studied. The prepared mixture exhibits a wide temperature interval of the CSm G phase, which presents a multi-domain, polycrystalline structure where each domain acts as a uniaxial crystal. Over time the domains merge, and a uniaxial, monodomain crystal with 3D symmetry, which is transparent in the visible and near-infrared ranges of the optical spectrum, is formed. Due to its high birefringence, the CSm G-based phase retarder is much thinner than the most commonly used phase retarder, such as the quartz-based one. In addition, we have shown several examples of the possible use of CSm G phase retarders, such as spatial-temporal modulation of two collinear laser beams, solar spectral radiation division, and aerospace applications. Moreover, the proposed CSm G phase retarder can be used in many directions such as optical chemical analysis, medicine, environmental monitoring, astronomy, and polarimetry.

Acknowledgments

This work is supported by Shota Rustaveli National Science Foundation of Georgia, project number YS 21-128.

References

[1] Vargas, J.; Uribe-Patarroyo, N.; Quiroga, J.A.; Alvarez-Herrero, A.; Belenguer T. Optical inspection of liquid Crystal Variable Retarder Inhomogeneities. *Appl. Opt*. **2010**, *49*, 568–574. http://dx.doi.org/10.1364/AO.49.000568
[2] Kemp, J.C.; Piezo-Optical Birefringence Modulators: New Use for a Long-Known Effect. *J. Opt. Soc. Am*. **1969**, *59*, 950–953. https://doi.org/10.1364/JOSA.59.000950
[3] Saleh, B.E.A.; Teich, M.C. *Fundamentals of Photonics*. 2nd Edition; Wiley-Interscience, 2007. ISBN-10: 0471358320.
[4] Cao, W.; Yang, X.; Gao, J. Broadband Polarization Conversion with Anisotropic Plasmonic Metasurfaces. *Sci. Rep*. **2017**, *7*, 8841. https://doi.org/10.1038/s41598-017-09476-8
[5] Lavrentovich, M.D.; Sergan, T.A.; Kelly, J.R. Switchable Broadband Achromatic Half-Wave Plate with Nematic Liquid Crystals. *Opt. Lett*. **2004**, *29*, 1411–1413. https://doi.org/10.1364/OL.29.001411
[6] Zhuang, Z.; Kim, Y.J.; Patel, J.S. Achromatic Linear Polarization Rotator Using Twisted Nematic Liquid Crystals. *Appl. Phys. Lett*. **2000**, *76*, 3995–3997. https://doi.org/10.1063/1.126846
[7] Wu, Th. X.; Huang, Y.; Wu, S.-T. Design Optimization of Broadband Linear Polarization Converter Using Twisted Nematic Liquid Crystal. *Jpn. J. Appl. Phys*. **2003**, *42*, L39. https://doi.org/10.1143/JJAP.42.L39
[8] Bueno, J.M. Polarimetry Using Liquid-Crystal Variable Retarders: Theory and Calibration. *J. Opt. A: Pure Appl. Opt*. **2000**, *2*, 216–222. https://doi.org/10.1088/1464-4258/2/3/308
[9] Ren, H.; Fan, Y.H.; Lin, Y.H.; Wu, S.T. Tunable-Focus Microlens Arrays Using Nanosized Polymerdispersed Liquid Crystal Droplets. *Opt. Commun*. **2005**, *247*, 101–106. https://doi.org/10.1016/j.optcom.2004.11.033
[10] Liu, C.Y.; Chen, L.W. Tunable Photonic-Crystal Waveguide Mach-Zehnder Interferometer Achieved by Nematic Liquid-Crystal Phase Modulation. *Opt. Express* **2004**, *12*, 2616–2624. https://doi.org/10.1364/OPEX.12.002616
[11] Hahn, J.; Kim, H.; Lim, Y.; Park, G.; Lee, B. Wide Viewing Angle Dynamic Holographic Stereogram with a Curved Array of Spatial Light Modulators. *Opt. Express* **2008**, *16*, 12372–12386. https://doi.org/10.1364/OE.16.012372
[12] Apter, B.; Efron, U.; Bahat-Treidel, E. On the Fringing-Field Effect in Liquid-Crystal Beam-Steering Devices. *Appl. Opt*. **2004**, *43*, 11–19. https://doi.org/10.1364/AO.43.000011
[13] Yang, D.K.; Wu, S.T. *Fundamentals of Liquid Crystal Devices*. John Wiley & Sons, Ltd. 2006. ISBN: 0-470-01542-X.
[14] Rajasekharan-Unnithan, R.; Butt H.; Wilkinson T.D. Optical Phase Modulation Using a Hybrid Carbon Nanotube-Liquid-Crystal Nanophotonic Device. *Opt. Lett*. **2009**, *34*, 1237–1239. https://doi.0146-9592/09/081237-3/$15.00
[15] Nicolás, J.; Campos, J.; Yzuel, M.J. Phase and Amplitude Modulation of Elliptic Polarization States by Nonabsorbing Anisotropic Elements: Application to Liquid-Crystal Devices. *J. Opt. Soc. Am. A*. **2002**, *19*, 1013–1020. https://doi.org/10.1364/JOSAA.19.001013
[16] Vargas, J.; Uribe-Patarroyo, N.; Quiroga, J.A.; Alvarez-Herrero, A.; Belenguer T. Optical Inspection of Liquid Crystal Variable Retarder Inhomogeneities. *Appl. Opt*. **2010**, *49*, 568–574. https://doi.org/10.1364/AO.49.000568
[17] Fuh, A. Y.-G.; Chiang, J.-T.; Chien, Yu-Sh.; Chang, Ch.-J.; Lin, H.-Ch. Multistable Phase-Retardation Plate Based on Gelator-Doped Liquid Crystals. *Appl. Phys. Express* **2012**, *5*, 072503. http://dx.doi.org/10.1143/APEX.5.072503
[18] Safrani, A.; Abdulhalim, I. Liquid-Crystal Polarization Rotator and a Tunable Polarizer. *Opt. Lett*. **2009**, *34*, 1801–1803. https://doi.org/10.1364/OL.34.001801
[19] Petriashvili, G.; Chanishvili, A.; Wardosanidze, Z. Cholesteric Liquid Crystal Mirror Based Imaging Stokes Polarimeter. *Appl. Opt*. **2021**, *60*, 3187–3191. https://doi.org/10.1364/AO.422814
[20] Schnoor, N.P.; Niemeier, R.C.; Woods, A.L.; Rogers, J.D. Calibration of Liquid Crystal Variable Retarders Using a Common-Path Interferometer and Fit of a Closed-Form Expression for the Retardance Curve. *Appl. Opt*. **2020**, *59*, 10673–10679. https://doi.org/10.1364/AO.408383
[21] Demchuk, Y.; Gunka, V.; Pyshyev, S.; Sidun, Y.; Hrynchuk, Y.; Kucinska-Lipka, J.; Bratychak, M. Slurry Surfacing Mixed on the Basis of Bitumen Modified with Phenol-Cresol-Formaldehyde Resin. *Chem. Chem. Technol*. **2020**, *14*, 251–256. https://doi.org/10.23939/chcht14.02.251
[22] Mukbaniani, O.; Tatrishvili, T.; Kvinikadze, N.; Bukia, T.; Pachulia, Z.; Pirtskheliani, N.; Petriashvili, G. Friedel-Crafts Reaction of Vinyl Trimethoxysilane with Styrene and Composite Materials on Their Base. *Chem. Chem. Technol*. **2023**, *17*, 325–338. https://doi.org/10.23939/chcht17.02.325
[23] Iatsyshyn, O.; Astakhova, O.; Shyshchak, O.; Lazorko O.; Bratychak, M. Monomethacrylate Derivative of ED-24 Epoxy Resin and its Application. *Chem. Chem. Technol*. **2013**, *7*, 73–77. https://doi.10.23939/chcht07.01.073
[24] Hanna, J.-I.; Ohno, A.; Iino, H. Charge Carrier Transport in Liquid Crystals. *Thin Solid Films* **2014**, *554*, 58–63. https://doi.10.1016/j.tsf.2013.10.051

[25] Baron, M.; Stepto, R.F.T. Definitions of Basic Terms Relating to Low-Molar-Mass and Polymer Liquid Crystals. *Pure Appl. Chem*. **2002**, *74*, 493–509. https://doi.10.1351/pac200274030493
[26] Espinet, P.; Esteruela, M.A.; Ore, L.A.; Serrano, J.L.; Sola, E. Transition Metal Liquid Crystals: Advanced Materials within the Reach of the Coordination Chemist. *Coord Chem Rev* **1992**, *117*, 215–274. https://doi. 10.1016/0010-8545(92)80025-M
[27] Niezgoda, I.; Jaworska, J.; Pociecha, D.; Galewski, Z. The Kinetics of the E-Z-E Isomerisation and Liquid-Crystalline Properties of Selected Azobenzene Derivatives Investigated by the Prism of the Ester Group Inversion. *Liq Cryst* **2015**, *42*, 1148–1158. https://doi.10.1080/02678292.2015.1031198
[28] Obadovic, D.Z.; Stojanovic, M.; Bubnov, A.; Eber, N.; Cvetinov, M.; Vajda, A. Structural Studies on Different Types of Ferroelectric Liquid Crystalline Substances. *Journal of Research in Physics* **2011**, *35*, 3–13. http://dx.doi.org/10.2478/v10242-012-0001-3

Received: August 25, 2023 / Revised: September 05, 2023 / Accepted: September 29, 2023

КРИСТАЛІЧНИЙ СМЕКТИЧНИЙ G-ФАЗОВИЙ СПОВІЛЬНЮВАЧ ДЛЯ ПРОСТОРОВО-ЧАСОВОЇ МОДУЛЯЦІЇ ОПТИЧНОЇ ІНФОРМАЦІЇ В РЕАЛЬНОМУ ЧАСІ

Анотація. *Виготовлено та досліджено новий фазовий сповільнювач на основі рідкісної та маловивченої рідкокристалічної фази – кристалічної смектичної G-фази, отриманої змішуванням двох сертифікованих нематичних сумішей. Фазовий сповільнювач прозорий у видимій і ближній інфрачервоній частинах оптичного спектру. Температурна стабільність у широкому діапазоні температур, високе двозаломлення та висока міцність дають змогу виготовляти різні типи сповільнювачів фаз, які можна використовувати в оптиці, оптико-хімічному аналізі та поляриметрії.*

Ключові слова: *кристалічна смектична G-фаза, фазовий сповільнювач, оптична інформація.*